International Journal of Computer Information Systems and Industrial Management Applications
ISSN 2150-7988 Volume 17 (2025) pp. 1-19

https://doi.org/10.70917/ijcisim-2025-0213
Article

Research on Cost-Effectiveness Analysis of Concrete Materials Based on Optimization Algorithm

Jun Shen [1], Xuejun Xiao [2,3,*] and Yuehao Ye [4]

[1] School of Electromechanical and Automotive Engineering, Qingyuan Polytechnic, Qingyuan, Guangdong, 511510, China
[2] School of Chemical and Pharmaceutical Engineering, Changzhou Institute of Engineering Technology, Changzhou, Jiangsu, 213164, China
[3] School of Mining Engineering, China University of Mining and Technology, Xuzhou, Jiangsu, 221116, China
[4] Shenzhen Pengcheng Foundation Concrete Co., Ltd., Shenzhen, Guangdong, 518118, China; xxjcj198109@163com

Abstract: Concrete, as an important construction material in modern construction projects, is widely used in various fields of engineering and plays a great role in it, and different types of concrete have different impacts on project costs. The study adopts Box-Behnken experimental design method in response surface methodology to establish a response surface test model with water-cement ratio, recycled brick aggregate substitution rate, and polypropylene fiber volume fraction as factors. Meanwhile, an objective function considering economic cost and carbon emission is constructed, and an improved non-dominated sequential genetic algorithm (I-NSGA-II) is proposed for the optimal design method of concrete proportion. The results show that the testing model is well fitted with high prediction accuracy; for flexural strength, split tensile strength and compressive strength, the corresponding optimal BF admixtures are 0.2%, 0.1% and 0.2%, respectively. After testing, the improved algorithm significantly improves the speed of convergence and the uniformity of the distribution of optimal solutions. Finally, the multi-objective optimization model proposed in this paper is applied to concrete cost analysis, and 10 sets of optimal mixes are found among 200 sets of mixes by Topsis method. The objective function range is used as a constraint to establish a constrained multi-objective optimization model to find 10 groups of optimal fit ratios by the same method, and comparing the two types of optimal fit ratios, the multi-objective optimization model in this paper can obtain a higher Topsis score.

Keywords: response surface method; multi-objective optimization; NSGA-II; concrete

1. Introduction

Concrete material is a man-made stone composed of cement, aggregate, sand, water and admixture. Concrete is a widely used material in construction projects, which is characterized by high strength, durability, easy availability of raw materials, easy processing and low cost, and since its invention, human beings have used it to construct many breathtaking buildings, such as the Eiffel Tower and the Yangtze River Bridge, which has become an irreplaceable cornerstone material in the construction industry [1-3]. With the acceleration of urbanization and the rapid development of the construction industry, the use of concrete in the global construction materials accounts for more than 70%, in response to the market demand and the call for low-carbon policies, the development of concrete materials is also gradually moving towards the functionalization and greening, materials such as Ultra-High Performance Concrete (UHPC) and environmentally friendly concrete have been developed, and the performance of different types of concrete materials varies, and there are differences in cost-effectiveness [4-8]. And the cost of concrete materials is closely related to the quality of material production and the cost and quality of construction projects, so there is an increasing competition among concrete material manufacturers

[9-10].

Product cost-benefit analysis is an important part of enterprise and product management, through the cost-benefit analysis, to find the concrete production management loopholes, to provide various cost information for concrete production, so as to reduce the cost, to formulate concrete improvement measures, and to make the right decision [11-14]. Based on the full life cycle cost (LCC) theory, the cost of concrete can be divided into four areas, namely, direct cost (raw materials, production process), indirect cost (construction efficiency, transportation), environmental cost (carbon emission, waste reuse), and maintenance cost (performance enhancement, restoration) [15-19]. Adamu and Ibrahim [20] used the response surface methodology to analyze the cost of concrete materials blended with date ash and eggshell powder concrete materials for environmental sustainability analysis and its cost-benefit analysis using carbon dioxide emission as an environmental cost indicator, the results of the analysis gave a low-cost and environmentally friendly concrete formulation i.e. 21.3% date palm ash and 2.3% eggshell powder. Jhatial et al [21] used carbon footprint and eco-strength efficiency in the assessment of the sustainability of concrete incorporated with eggshell powder as assessment indicator, while cost effectiveness was assessed using total cost and production cost per unit of compressive strength. Makul et al [22] constructed a cost-benefit analysis model for concrete with recycled aggregates, which adequately assessed the cost impact of concrete production with recycled aggregates, including information on the type of plant production facilities, concrete supply and demand, and material pricing.

With the application and development of artificial intelligence technology, intelligent algorithms are applied to generate a variety of multi-objective optimization schemes and intelligent decision-making schemes, which are promising for material performance optimization and cost analysis optimization. Gheibi et al [23] used meta-heuristic genetic algorithms (GA) to conduct a life-cycle assessment of the concrete production process, which focuses on air pollutants and health risks during the production process, and can assist in the concrete production cost analysis. Naseri [24] used GA and Particle Swarm Optimization (PSO) algorithm to optimize the concrete design ratios, which resulted in lowering the total cost of the finished material, while the PSO effect was slightly higher than that of GA. Gao et al. [25] for evaluating the LCC of new materials and technologies for construction used a comprehensive bottom-up approach based on the LCC to evaluate the performance of the materials and technologies, their maintenance and rehabilitation schedules and introduced a meta-heuristic evolutionary algorithm to determine the optimal investment plan for LCC analysis. Tavares and Grassley [26] utilized a hybrid design tool based on machine learning algorithms to predict the UHPC compressive strengths, and generated cost and environmental efficiency density maps by combining the environmental factors and the unit cost to achieve the minimization of the carbon footprint and cost of the UHPC. Aydın et al [27] Developed a predictive neural network model through meta-heuristic optimization algorithm for evaluating carbon emissions during alkali-activated concrete production, in which the GA algorithm performed the best. Haigh et al [28] analyzed the economic cost and GHG emissions of concrete material fabrication based on recycled waste cardboards through a non-dominated sorting GA method, and the results showed that the increase in the fabrication process and the cost of the materials resulted in a higher overall fabrication cost. Ahmadi-Nedushan and Almaleeh [29] analyzed the cost of individual reinforced concrete materials based on ACI 318-19 standard using elite GA and combined with sensitivity analysis to optimize the design to reduce the material cost. Lv et al [30] constructed an artificial neural network based performance prediction model for UHPC and used a machine learning algorithm for performance comparison, and achieved a cost reduction of $776/m3 by GA under consideration of UHPC proportioning mass, proportion ratio, and absolute volume constraints. Elmasry and Elshaarawy [31] optimized the CatBoost algorithm using three hybrid meta-heuristic optimization algorithms, and designed a graphical user interface for estimating concrete solid slab construction cost.

This paper takes concrete materials as the research object and combines the response surface method and the improved NSGA-II algorithmic model for cost-benefit analysis. Firstly, the response surface method is applied for experimental design, and the water-cement ratio, recycled brick aggregate substitution rate, and volume fraction of polypropylene fibers are taken as factors, and flexural strength, compressive strength, and abrasion are taken as evaluation indexes for the regression model analysis, and meanwhile, the effects of the length of fibers (BF) and the volume admixture on the mechanical properties of fiber-recycled concrete are analyzed. Based on the multi-objective optimization theory, an improved non-dominated sorting genetic algorithm for optimal design of concrete mix ratio is proposed to optimize the mix ratio with economic cost and carbon emission as the objective function. Typical test functions are selected to test the improved NSGA-II algorithm, analyze the solution speed and accuracy of the test algorithms, and compare their optimization results, so as to provide more choices and practical operability for the actual projects.

2. Concrete material proportioning design experiment

2.1. Response surface methodology

Response surface methodology is a method to solve multivariate problems by reasonably utilizing experimental design methods, obtaining data through experimental validation, and fitting the functional relationship between factors and response values using multivariate quadratic regression equations in order to find the optimal process parameters [32]. Commonly used response surface methods include CCD (Center Composite Design) and BBD (Box Behnken Design). Among them, the CCD method can be applied to the experimental design of three factors, and accurately predict the nonlinear relationship between the factors through multiple trials; the BBD method can predict the nonlinear relationship between the factors without conducting multiple trials. Meanwhile, the BBD method has a high level of restriction on the factors, and three levels of each factor can be selected (high level, coded value of 1; medium level, coded value of 0; low level, coded value of -1), so that the factor changes do not exceed the safety range. Therefore, taking all considerations into account, this paper applies the response surface BBD method to establish the regression model. The response value formula is expressed as:

$$Y = \beta_0 + \sum_{i=1}^{n}\left(\beta_i x_i\right) + \sum_{i=1}^{n}\left(\beta_{ii} x_i^2\right) + \sum_{i=1}^{n}\sum_{j=1}^{n}\left(\beta_{ij} x_i x_j\right) + \varepsilon \tag{1}$$

In the formula, β_0 denotes the constant term; x_i, x_j all denote independent variables; β_i denotes the primary term coefficient; β_i denotes the secondary term coefficient; β_{ij} denotes the interaction term coefficient; ε denotes the random error; and n denotes the number of variables.

Since the primary term coefficient, secondary term coefficient, and interaction term coefficient are the main factors affecting the prediction results of the model, in order to improve the credibility of the model, the reliability of the model needs to be assessed by the correlation coefficient and the adjustment coefficient. The correlation coefficient R^2 formula is expressed as:

$$R^2 = 1 - \frac{S_\tau}{S_m + S_\tau} \tag{2}$$

$$R_a^2 = \frac{S_\tau / D_\tau}{\left(S_m + S_\tau\right)/\left(D_m + D_\tau\right)} \tag{3}$$

where, S_τ represents the residual sum of squares; S_m represents the regression sum of squares; D_τ represents the residual degrees of freedom; and D_m represents the regression degrees of freedom.

Since the center point represents the number of repetitions of the test, the calculation of the center point can effectively reduce the error of the test prediction results, so, in the later concrete material proportion test, the center point needs to be calculated. In this paper, Design-expert 8.0.6 software is applied to calculate and give the center point.

2.2. Experimental design

2.2.1. Raw materials

① Cement: P-O42.5 ordinary silicate cement, density 3.2g/cm^3, specific surface area 371m^2/kg, 28d unconfined compressive strength of 45.6MPa. ② Recycled Coarse Aggregate: taken from an urban area of A reconstruction project, the old mortar adhesion rate of about 20.0%, density 2.6g/cm^3, water absorption of 5.6%, crushing value of the index 15.6%, porosity 43.2%. ③ Natural coarse aggregate: limestone crushed stone, gradation 5~25mm, water absorption 1.09%, crushing value index 4.6%, porosity 39.8%. ④ River sand: fineness modulus 2.6, Zone II medium sand. ⑤ Polypropylene fiber: average diameter 0.05mm, average length 20mm, tensile strength 323MPa, modulus of elasticity 3400MPa, ultimate elongation 18%. ⑥ All water used is tap water. ⑦ The water reducing agent is polycarboxylic acid system high performance water reducing agent.

2.2.2. Mixing ratio design

The design of the mix ratio is based on the Box-Behnken principle of response surface methodology, and the water-cement ratio, recycled aggregate mass substitution rate and fiber volume admixture are selected as test variables to determine the optimum mix ratio for recycled concrete. The three independent variables selected for the study were named as A (water-cement ratio 0.4-0.6), B (recycled

coarse aggregate substitution rate 50%-90%), and C (fiber volume admixture 0-0.1%). The different independent variable factors were imported into the DesignExport software to obtain the fit ratios for 17 sets of tests (5 sets of replicated tests including the center point were used to calculate the error).

2.2.3. Test Methods

The concrete was prepared by referring to the experience of pre-mixing in the project, firstly, after mixing the dry cement and aggregate evenly, adding polypropylene fibers slowly in layers and gradually pouring in the liquid components, and continuously mixing until the consistency of the slurry was uniform. The slump test was conducted according to GB/T50080-2016 Standard for Test Methods of Properties of Ordinary Concrete Mixes. Cubic specimens with a side length of 100mm and 160mm×160mm×40mm prismatic specimens were produced respectively, and the unconfined compressive strength was determined after 28d of curing in a standard curing box, and the operation procedure was carried out according to GB/T50081-2019 Standard for Test Methods of Physical and Mechanical Properties of Concrete.

2.3. Results and analysis

2.3.1. Response surface modeling and testing

(1) Model building

Based on the principle of least squares regression analysis of the test results, the HFRAC flexural strength, compressive strength and wear prediction models were obtained, as shown in Eqs. (4)~(6), respectively:

$$y_1 = -347.015 + 6.2825x_1 + 15.82x_2 + 19.05063x_3 + 1.93x_1x_2 + 0.035x_1x_3 - 0.3125x_2x_3 - 4.35x_1^2 - 3.48x_2^2 - 0.260625x_3^2 \tag{4}$$

$$y_2 = -559.75 - 6.105x_1 + 21.645x_2 + 32.4075x_3 - 2.4x_1x_2 + 0.175x_1x_3 - 0.325x_2x_3 + 2.54x_1^2 - 3.46x_2^2 - 0.4475x_3^2 \tag{5}$$

$$y_3 = 25.58 - 3.0182x_1 - 2.2112x_2 - 1.20458x_3 + 0.265x_1x_2 + 0.02275x_1x_3 + 0.02075x_2x_3 + 0.9101x_1^2 + 0.4561x_2^2 + 0.016631x_3^2 \tag{6}$$

where: y_1 is the 28d flexural strength; y_2 is the 28d compressive strength; y_3 is the abrasion; x_1 is the SF volume admixture; x_2 is the MPPF volume admixture; and x_3 is the sand rate.

(2) Model checking

In order to estimate the accuracy and validity of the above models, ANOVA was performed on each regression model and the test results are shown in Tables 1-3. The model significance was tested by F -test and the F -value was calculated as shown in equation (7).

$$F = \frac{M_r}{M_e} = \frac{S_r / \nu}{S_e / (n - \nu - 1)} \tag{7}$$

where: M_r is the mean square of regression; M_e is the mean square of residuals; S_r is the sum of squares of regression; S_e is the sum of squares of residuals; n is the number of experimental groups; ν is the number of variables in the response model.

The F -value is greater than the critical value F_0, indicating that the model is valid and statistically significant. P -value represents the probability of $F < F_0$, i.e., based on the P -value, the significance of each of the models can be assessed. When $P < 0.01$ is highly significant, when $0.01 \bullet P \bullet 0.05$ is significant, and when $P > 0.05$ is not significant.

From Table 1-Table 3, it can be seen that: the P-value of each model is less than 0.01, which indicates that the models are highly significant, reliable and statistically significant; the P-value of the out-of-fit term is greater than 0.05, which indicates that the models are well fitted. The model correction coefficients of determination were 0.9725, 0.9645, and 0.9655, indicating that the models explained 97.25%, 96.45%, and 96.55% of the variation in response values, respectively. The model prediction

coefficients of determination were 0.9458, 0.9128, 0.8437, with coefficients of variation (C.V.) less than 10%, and signal-to-noise ratios much greater than 4, indicating that the models have a high degree of fit with the actual, and that the above models can be used for the optimization of the subsequent analysis.

Table 1. Variance analysis of the regression model of y_1.

Source	Degree of freedom	Sum df square	Mean square	F value	P value
Model	9	17.19	1.95	55.78	<0.0001
x_1	1	1.25	1.23	34.82	0.0008
x_2	1	0.4472	0.4472	12.05	0.0109
x_3	1	0.0026	0.0026	0.0615	0.8258
x_1x_2	1	0.9551	0.9551	28.57	0.0016
x_1x_3	1	0.0053	0.0053	0.1479	0.7214
x_2x_3	1	0.4142	0.4142	11.74	0.0131
x_1^2	1	5.004	5.004	143.05	<0.0001
x_2^2	1	3.24	3.24	91.18	<0.0001
x_3^2	1	4.64	4.64	131.38	<0.0001
Residual	8	0.2713	0.0362		
Lack of fit	4	0.0453	0.0413	0.2605	0.8574
Cor total	17	17.44			

Note: adjusted R^2=0.9725, predicted R^2=0.9458, C.V.=3.34%, adequate precision=21.2308.

Table 2. Variance analysis of the regression model of y_2.

Source	Degree of freedom	Sum df square	Mean square	F value	P value
Model	9	37.86	4.28	37.29	<0.0001
x_1	1	16.67	16.67	146.56	<0.0001
x_2	1	0.8212	0.8212	7.09	0.0343
x_3	1	0.0468	0.0468	0.5685	0.5629
x_1x_2	1	1.58	1.58	12.92	0.0095
x_1x_3	1	0.1329	0.1329	1.25	0.3429
x_2x_3	1	0.4625	0.4625	3.91	0.0953
x_1^2	1	1.84	1.84	15.2	0.0064
x_2^2	1	3.29	3.29	28.07	0.0015
x_3^2	1	13.63	13.63	119.63	0.0011
Residual	8	0.8305	0.1285		
Lack of fit	4	0.2125	0.0754	0.3523	0.8129
Cor total	17	38.66			

Note: adjusted R^2=0.9645, predicted R^2=0.9128, C.V.=1.14%, adequate precision=19.1795.

Table 3. Variance analysis of the regression model of y_3.

Source	Degree of freedom	Sum df square	Mean square	F value	P value
Model	9	0.5844	0.0651	38.74	<0.0001
x_1	1	0.0287	0.0277	16.58	0.0062
x_2	1	0.1787	0.1664	99.32	<0.0001
x_3	1	0.0563	0.044	26.37	0.0017
x_1x_2	1	0.0316	0.0193	11.52	0.0152

x_1x_3	1	0.0161	0.0038	1.29	0.3124
x_2x_3	1	0.0157	0.0034	1.09	0.3515
x_1^2	1	0.232	0.2197	132.57	<0.0001
x_2^2	1	0.0687	0.0564	34.79	0.0009
x_3^2	1	0.0326	0.0203	12.09	0.0131
Residual	8	0.0257	0.0034		
Lack of fit	4	0.0195	0.0035	1.28	0.4328
Cor total	17	0.5961			

Note: adjusted R^2 = 0.9655, predicted R^2=0.8437, C.V. = 2.14%, adequate precision = 22.1856.

From the analysis of variance, it can be seen that: SF volume doping has a highly significant effect on flexural strength, compressive strength and wear; MPPF volume doping has a highly significant effect on wear and tear, and a significant effect on flexural and compressive strength; sand rate has a highly significant effect on wear and tear. From the interaction effects, it can be seen that: SF volume doping and MPPF volume doping interacted with each other to have highly significant effects on flexural and compressive strengths, and significant effects on the amount of abrasion; MPPF volume doping interacted with the sand rate to have significant effects on flexural strengths.

2.3.2. Analysis of model results

The RSM scheme was imported into Design Expert software and the relevant models were established to analyze the significant degree of the effects of fiber (BF) length and volume doping and their interactions on the strength response based on the three-dimensional response surface plots and contour plots obtained from the model fitting of flexural strength, split tensile strength, and compressive strength as shown in Figs. 1 and 2.

For the flexural strength, it can be seen from Figs. 1(a) and 2(a) that: (i) the three-dimensional response surface plots show that the surface trend along the axis of BF volume doping is steeper, while the surface trend along the axis of bf length is more gentle, i.e., for the flexural strength, the effect of BF volume doping is more prominent; (ii) the contour plots of the contours in the longitudinal coordinate are more intensive than the contour plots in the transverse coordinate, which indicates that the effect of bf volume doping on the flexural strength is more prominent than the one of BF length. bf volume doping has a greater effect on flexural strength than BF length.

For the split tensile strength, it can be seen from Figs. 1(b) and 2(b) that: (i) the three-dimensional response surface shows that the surface trend along the axes of BF volume doping and length are relatively smooth, i.e., the influence of BF volume doping and length on the split tensile strength is relatively similar; (ii) the contour plots of the transverse and longitudinal coordinates of the contour lines are similarly dense, which indicates that the influence of BF volume doping and length on the split tensile strength is similar. to a similar extent.

For the compressive strength, it can be seen from Figs. 1(c) and 2(c) that: ① the three-dimensional response surface shows that the surface trend along the axis of BF length is steeper, while the surface trend along the axis of BF volume doping is smoother, i.e., the effect of BF length on the compressive strength is more significant; ② the degree of intensity of contour lines on the transverse coordinate of the contour map is greater than that on the longitudinal coordinate, indicating that the effect of BF length on the compressive strength is greater than that on BF length, and that the effect of BF length on the compressive strength is more than that on BF length. compressive strength is greater than that of BF volume doping.

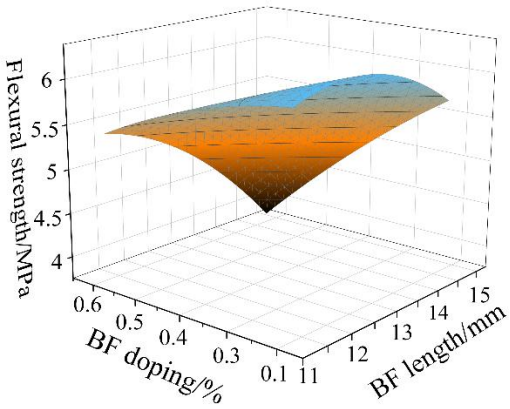

(a) Flexural strength

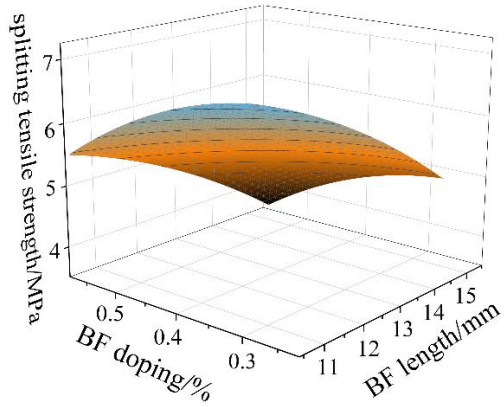

(b) Split tensile strength

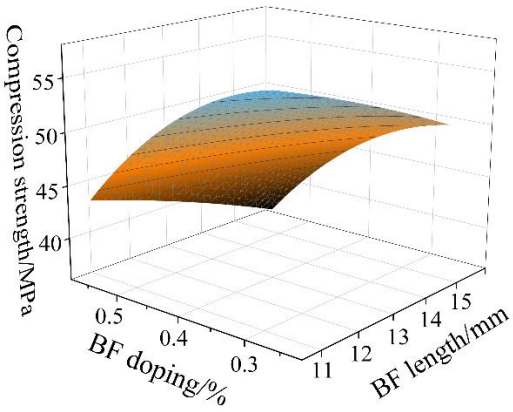

(c) Compression strength

Figure 1. Three-dimensional response surface of mechanical properties.

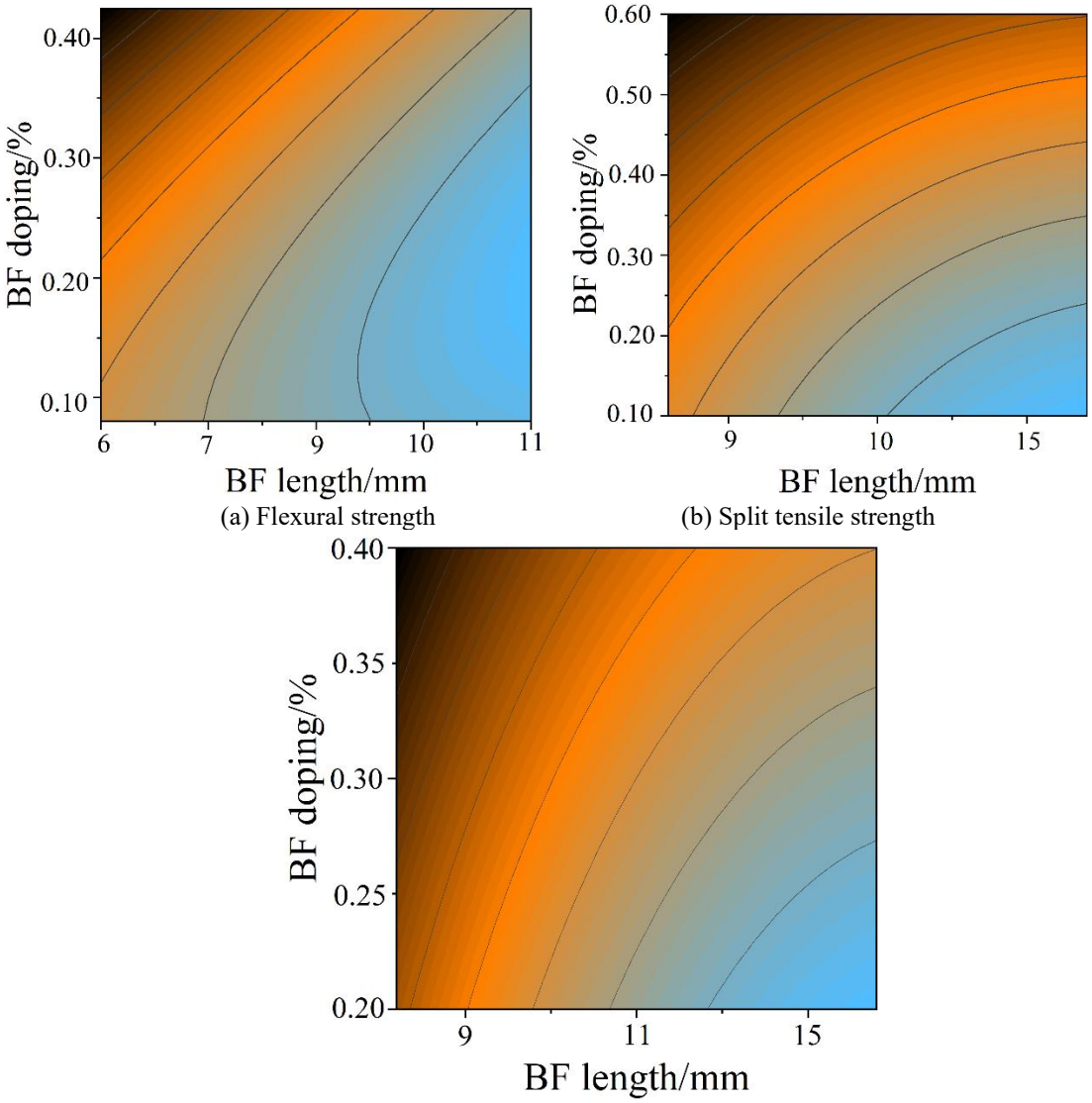

(a) Flexural strength (b) Split tensile strength

(c) Compression strength

Figure 2. Mechanical properties contour map.

3. Improved NSGA-II model for cost-effective optimization of concrete materials

3.1. Objective function considering economic costs and carbon emissions

3.1.1. Multi-objective optimization problem

The objective optimization problem generally refers to obtaining the optimal solution of the objective function under certain constraints and through certain optimization algorithms. When the optimization objective function is one, it is called single-objective optimization, and when there are two or more objective functions, it is called multi-objective optimization. Unlike single-objective optimization where the solution is finite, multi-objective optimization optimizes the solution. Multi-objective optimization should firstly solve the problem of existence of the solution, and secondly solve how to solve the problem. The mathematical model of multi-objective optimization is:

$$\min f_i\left(x_1, x_2, \cdots, x_n\right) i = 1, 2, \cdots, s \tag{8}$$

$$s.t. g_i\left(x_1, x_2, \cdots, x_n\right) = 0 i = 1, 2, \cdots, m \tag{9}$$

Multi-objective optimization algorithms are summarized in two categories: traditional optimization algorithms and intelligent optimization algorithms. Traditional optimization algorithms include ideal point method, weighting method, constraint method, linear programming method, etc., which essentially transforms the multi-objective function into a single-objective solution. Intelligent optimization

algorithms include evolutionary algorithms, particle swarm algorithms, etc., which can obtain more Pareto solutions, which constitute an optimal solution set, also known as Pareto frontier.

3.1.2. Selection of Optimization Objectives

Under the premise of meeting the performance requirements, the economic cost and carbon emissions as the objective function, the obtained ratio space to seek the optimal ratio parameters of the economic cost and carbon emissions are smaller. The reasons for establishing the objective function on the fit ratio parameter (m,n,l) with economic cost and carbon emission respectively are as follows:

(1) The reality of engineering construction requires that the economic cost and carbon emission of the asphalt concrete core wall be controlled, so that the use of the fit ratio parameter meets the basic performance requirements, and at the same time, achieves the purpose of cost reduction, energy saving and emission reduction.

(2) Due to the special characteristics of hydraulic asphalt concrete preparation, hot mix asphalt mixture of aggregate and asphalt need to be heated to 170 ℃, to ensure that it has the mobility to cover the aggregate, which will inevitably bring a lot of fuel consumption and carbon emissions, taking into account the large number of construction of pumped storage power stations in recent years, so there is a need to carry out the asphalt concrete ratio of economic analysis and quantitative analysis of carbon emissions.

(3) In the seepage control program selection, through the asphalt concrete seepage control wall economy and low-carbon quantitative analysis, for the use of asphalt concrete seepage control program to provide reference.

3.1.3. Establishment of the objective function

Taking filler concentration (m), aggregate ratio (n), and fine aggregate rate (l) as the decision variables of the double objective function of economic cost and carbon emission, the components of asphalt concrete are: assuming that the mass of asphalt A_1 is 1kg, the mass of filler A_2 is $m$kg, the mass of fine aggregate A_3 is $l(1+m)/n\mathrm{kg}$, and the mass of coarse aggregate A_4 is $(1-l)(1+m)/n\mathrm{kg}$.

Filler concentration and aggregate ratio are selected as the decision variables of the objective function because they are based on the theory of “mortar”, which better reflects the relationship between “component one structure and property”. theory to better reflect the relationship between “components, structure and performance”. The fine aggregate ratio was chosen as another decision variable because it is more intuitive to show the composition of aggregates, and it is more convenient to convert it into fine aggregate and coarse aggregate quality when establishing the objective function of asphalt concrete economy and low carbon performance. The m,n value interval is referred to the relevant technical specifications, and the l value interval is determined to be 30~60% by the grading curve verification test in Chapter III.

Asphalt concrete from the acquisition of raw materials to paving in the heart of the wall part of the whole process of carbon emissions include the use of raw materials from the production of raw materials, to the transportation of materials after the material is heated to the paving to the heart of the wall part of the direct and indirect carbon emissions include: (1) Indirect carbon emissions from various raw materials in the design and production of asphalt concrete; (2) Direct carbon emissions caused by diesel fuel consumption in heating asphalt, aggregate, mineral powder and other raw materials to the mixing temperature; (3) Direct carbon emissions from the use of machinery and equipment. Three parts of the carbon emissions in the production of raw materials and raw materials heating two parts of the main source of carbon emissions, preparation and paving process of the use of machinery and carbon emissions are relatively small, the relevant studies have pointed out that the transportation of materials to the construction site as well as the construction site of the carbon emissions generated by the energy consumption only accounted for only 2% of the total amount of carbon emissions and 1%, so some of the carbon emissions can be ignored. The formula for calculating the carbon emissions of asphalt concrete per unit asphalt mass can be summarized as follows:

$$CE = A_1 \times D_1 + A_2 \times D_2 + A_3 \times D_3 + A_4 \times D_4 + A_5 \times \left(D_5 + D_6 \right) \tag{10}$$

where: A_5 - the amount of diesel fuel consumed in the heating process of raw materials in asphalt concrete.

Asphalt concrete from raw material processing to obtain to paving in the heart of the wall parts of the

whole process of economic costs mainly include the cost of raw materials (including the cost of transportation to the site) and raw materials heated to the mixing temperature caused by the energy consumption costs, the preparation and paving asphalt concrete in the use of machinery and labor costs due to the same process is only related to the amount of asphalt concrete paving, so the unit of asphalt quality of asphalt concrete under the economic costs of machinery and Labor costs are negligible. Unit asphalt quality of asphalt concrete economic cost formula can be summarized as:

$$E = 5.6 \times A_1 + 0.65 \times A_2 + 0.5 \times A_3 + 18 \times A_4 + 9.92 \times A_5 \tag{11}$$

In the process of asphalt mixture production, the equipment used for heating and drying aggregates is the main source of fuel consumption, while the moisture content of aggregates is also an important indicator of energy consumption. The energy required in the aggregate heating process includes the energy consumption for partial heating of the aggregate and the energy consumption for heating and evaporation of the water in the aggregate, which is calculated by the formula shown below:

$$E_{\text{Bone}} = \left(c_w + c_q\right) \times \left(A_3 + A_4\right) \times 1\% \times \left(t_2 - t_1\right) + c_a \times \left(A_3 + A_4\right) \times \left(t_3 - t_1\right) \tag{12}$$

$$A_6 = \frac{E_{\text{Bone}}}{Q \times \eta_1 \times \eta_3} \tag{13}$$

$$E_B = c_p \times A_1 \times \left(t_3 - t_4\right) \tag{14}$$

$$A_7 = \frac{E_{\text{B}}}{Q \times \eta_1 \times \eta_2} \tag{15}$$

$$E_{\text{Mine}} = c_m \times A_2 \times \left(t_3 - t_1\right) \tag{16}$$

$$A_8 = \frac{E_{\text{Mine}}}{Q \times \eta_1 \times \eta_3} \tag{17}$$

$$A_5 = A_6 + A_7 + A_8 \tag{18}$$

$$CE = 0.119 + 0.147m + 0.0321\left(\frac{1+m}{n}\right) + 0.0006l\left(\frac{1+m}{n}\right) \tag{19}$$

$$E = 5.62 + 18.04m + 0.73\left(\frac{1+m}{n}\right) - 0.15l\left(\frac{1+m}{n}\right) \tag{20}$$

$$Opt\left(CE^{\min}, E^{\min}\right) \tag{21}$$

where:

t_1 --Temperature of aggregate before heating/°C.

t_2 --Temperature at which water vapor evaporates/°C.

t_3 --Mixing temperature of raw materials heated to asphalt/°C.

CE--Carbon emissions from asphalt concrete per unit asphalt mass.

E--Economic cost of asphalt concrete per unit asphalt mass.

E_{Bone} --Heat required to heat aggregate to mixing temperature.

m, n, l --Decision variables for asphalt concrete mix ratio optimization.

A_6 --The amount of diesel fuel required to partially heat the aggregate.

A_7 --Amount of diesel fuel required for heating of matrix asphalt.

A_8 --Amount of diesel fuel required for heating of mineral powder.

3.2. Improved Genetic Solution Algorithm for Undominated Sorting

3.2.1. Genetic Algorithms for Undominated Sorting with Elite Strategies

The existing Non-dominated Sorting Genetic Algorithm with Elite Strategies [33] (NSGA-II) is an effective method for solving multi-objective optimization problems. NSGA-II is shown below. Its algorithmic flow can be mainly divided into population initialization, crossover and mutation operators,

non-dominated sorting, congestion distance sorting, and selection operators. The core of the algorithm is mainly two sorting algorithms as well as the selection operator.

Genetic Algorithm Flow for Undominated Sorting with Elite Strategy:

Data: the number of individuals in the population N, the maximum number of iterations $maxGen$.

Result: the set of Pareto-optimal solutions.

Initialize the number of populations and set the number of population iterations $Gen = 1$.

while the current number of iterations $Gen <$ the set maximum number of iterations $\max Gen$ do.

Crossover and mutation of the current individuals are performed to produce offspring.

Evaluate the fitness of each individual and non-dominated sort the individuals by fitness.

Individuals in the same dominance sorting class are then sorted by crowding distance.

Retain the top 50% of individuals into the next generation.

Update the current Pareto optimal solution.

3.2.2. Genetic Algorithm for Undominated Sorting with Equation Constraints

The conventional NSGA-II algorithm has been proved to have high search efficiency in the case of less than five objective functions, and also has the characteristics of fewer hyperparameters and more stable results, which has been widely used in multi-objective optimization problems. However, for material design, multi-objective optimization is usually an optimization process with constraints. The common constraints are as follows:

(1) Due to the limitations of processing preparation, operating conditions, etc., the search accuracy of multiple objective parameters to be optimized is usually different, and this kind of constraints is called the search step constraints, and the definition of the multi-objective optimization problem with the search step constraints is as shown in Eq. 3.3.

$$\begin{aligned} &\max\ f_i(X), i = 1, 2, \ldots, k \\ &s.t. X = \left[x_1, x_2, \ldots, x_m\right] = K \odot \left[y_1, y_2, \ldots, y_m\right] = \left[k_1 * y_1, k_2 * y_2, \ldots, k_m * y_m\right] \end{aligned} \tag{22}$$

Here, k denotes the number of optimization objectives, and m is the number of parameters to be optimized. $\odot$ denotes the multiplication of the corresponding elements of two vectors. K is an m-dimensional vector, where the i-th element k_i denotes the search step for the i-th optimization parameter, y_i is an integer, and $x_i = k_i * y_i$ denotes its constraint relationship, i.e., the optimized result x_i should be an integer multiple of the corresponding parameter search step k_i.

(2) In the design of new materials, it is common to mix a variety of components with variable material content of each component element, but their total amount is fixed, and this type of constraint is called the component ratio constraint. The multi-objective optimization problem for the constituent ratio constraint is defined as shown in Eq. (23).

$$\begin{aligned} &\max\ f_i(X), i = 1, 2, \ldots, k \\ &s.t. X = \left[x_1, x_2, \ldots, x_m\right], x_i \geq 0, i = 1, 2, \ldots, m \\ &\sum_{i=0}^{m} x_i = constant \end{aligned} \tag{23}$$

Here k denotes the number of optimization objectives, m is the number of parameters to be optimized, and $constant$ is a constant representing the total number of allocation ratio constraints fixed.

3.2.3. Genetic Algorithm for Undominated Sorting with Preferences

Conventional NSGA-II calculations of congestion distance ordering require that individuals in the same layer be as widely dispersed as possible, but this is usually not consistent with the requirements of materials design. This is because in most cases, materials researchers have an “expectation” or “preference” for the optimization objective. In other words, prior to material design, the researcher has an expectation of the performance of the new material to be designed, rather than being completely blind. Therefore, the direction of the Pareto-optimal solution obtained by the algorithm is important. Based on the NSGA-II algorithm, this paper proposes an NSGA-II algorithm with preferences (NSGA-IIP), which can make the solution set gather as much as possible in the preferred direction while solving the Pareto

optimal solution. The preference direction is represented by the vector A, as shown in Eq. (24).

$$A = \left(A_1, A_2, \ldots, A_k \right)^T \tag{24}$$

Each value in the vector A represents the expectation on the corresponding objective function. For the problem of material design with preferences, the preferences can be added to the congestion distance calculation. Thus the improved congestion distance calculation procedure is shown in Eq. (25).

$$D_i = \alpha \times p\_dis + \sum_{m=1}^{n} \frac{f_m(i+1) - f_m(i-1)}{f_m^{\max} - f_m^{\min}} \tag{25}$$

In Eq. (24), α is the weighting factor used to balance preferences and individual dispersion, and the second half of the sum in Eq. (24) is the same as the traditional congestion distance calculation. The p_dis in the first half of the sum represents the degree of similarity between feasible solutions and preferences. The more similar the feasible solution is to the preference direction, the larger the value of p_dis is, i.e., the more likely it is to be retained by the elite strategy and enter the next generation. p_dis can be computed using different calculations depending on the user's definition of the degree of similarity between the feasible solution and the preference. In this paper, we define two specific ways of calculating the similarity measure between individuals and preferences.

3.3. Performance Test of Improved NSGA-II Algorithm

In order to test the computational efficiency of the improved algorithm proposed in the paper, the traditional ZDT series of test functions and the single-peak function from the standard test of the CEC2005 International Competition are used in this test. The description of the test functions is shown in Table 4.

NSGA-II algorithm and the improved NSGA-II algorithm (I-NSGA-II) both belong to the non-dominated genetic algorithm, when the algorithm is running, the crossover factor and the scaling factor are first preset with a default value, and then automatically adjusted subsequently, and in order to test the effect of the improvement, the two algorithms are endowed with the same initial conditions (number of populations, crossover probability, and variance probability), and the dimension of the F single-peak function is set to D=30, ZDT classical function dimension is set to D=50 (high-dimensional), the population size $N_P = 50$, the maximum number of evaluations is (iteration number * dimension) 1000 * D, the optimal value is calculated by multiple optimization searching, and the sum of the optimal values of the test function is obtained.

Table 4. Overview of test functions.

Question	Test function	Constraint condition
F_1	$F_1(\vec{x}) = \sum_{l=1}^{D} z_i^2 + f\_bias_1$ $\vec{z} = \vec{x} - \vec{o}$ $F_1(\vec{x}^*) = f\_bias_1 = -450$	$\vec{x} \in [-100,100]^D$, D = 50
F_2	$F_2(\vec{x}) = \sum_{i=1}^{D} \left(\sum_{j=1}^{i} z_j^2 \right)^2 + f\_bias_2$ $\vec{z} = \vec{x} - \vec{o}$ $F_2(\vec{x}^*) = f\_bias_2 = -450$	$\vec{x} \in [-100,100]^D$, D = 50
F_3	$F_3(\vec{x}) = \sum_{i=1}^{D} \left(10^6\right)^{\frac{i-1}{D-1}} z_i^2 + f\_bias_3$ $\vec{z} = \vec{x} - \vec{o}$ $F_3(\vec{x}^*) = f\_bias_3 = -450$	$\vec{x} \in [-100,100]^D$, D = 50
ZDT_1	$f_1(x_1) = x_1$	$0 \le x_i \le 1$ D = 30

	$f_2(x_2)=g\left(1-\sqrt{\frac{f_1}{g}}\right)$ $g(x)=1+9\sum_{i=2}^{D}\frac{x_i}{D-1}$	
ZDT_2	$f_1(x_1)=x_1$ $f_2(x_2)=g\left(1-\left(\frac{f_1}{g}\right)^2\right)$ $g(x)=1+9\sum_{i=2}^{D}\frac{x_i}{D-1}$	$0\le x_i\le 1$ D = 30
ZDT_3	$f_1(x_1)=x_1$ $f_2(x_2)=g\left(1-\sqrt{\frac{f_1}{g}}\right)-\left(\frac{f_1}{g}\right)\sin(10pi\cdot f_1)$ $g(x)=1+9\sum_{i=2}^{D}\frac{x_i}{D-1}$	$0\le x_i\le 1$ D = 30

(1) Convergence speed

After the comparison test, the simulation graphs are obtained as shown in Fig. 3 and Fig. 4, and the number of iterations to find the optimal point for different functions is recorded under the operation of the two algorithms as shown in Table 5. Thus comparing the convergence trend graphs of F1, F2 and F3, it can be seen that the convergence speed of the improved NSGA-II algorithm is higher, especially in the initial optimization search performance is especially obvious.

Comparison test for the three functions of ZDT, the Pareto optimal solution obtained by the improved NSGA-II algorithm has a better distribution, while the distribution of the optimal solution fronts obtained by the NSGA-II algorithm is concentrated in a certain place in the region, and is relatively sparse elsewhere, and in the case of the ZDT2 problem, the individual congestion of the improved NSGA -II algorithm has a lower degree of crowding of individuals, and the density of individuals is also more decentralized, and the distribution is more uniform.

Table 5. The number of times to search for the best value.

Function	F_1	F_2	F_3
NSGA-II	118	174	143
I-NSGA-II	102	115	100

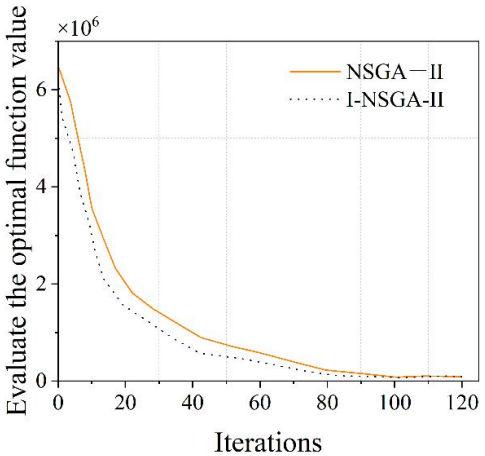

(a) F_1 function convergence curve

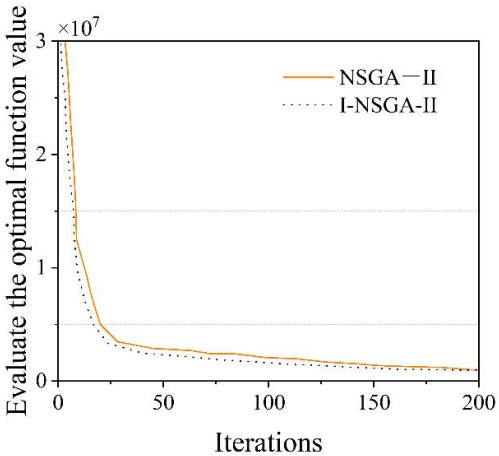

(b) F_2 function convergence curve

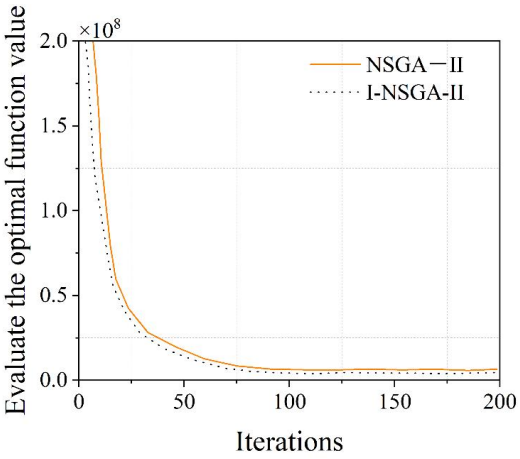

(c) F_3 function convergence curve

Figure 3. Comparison of convergence curves.

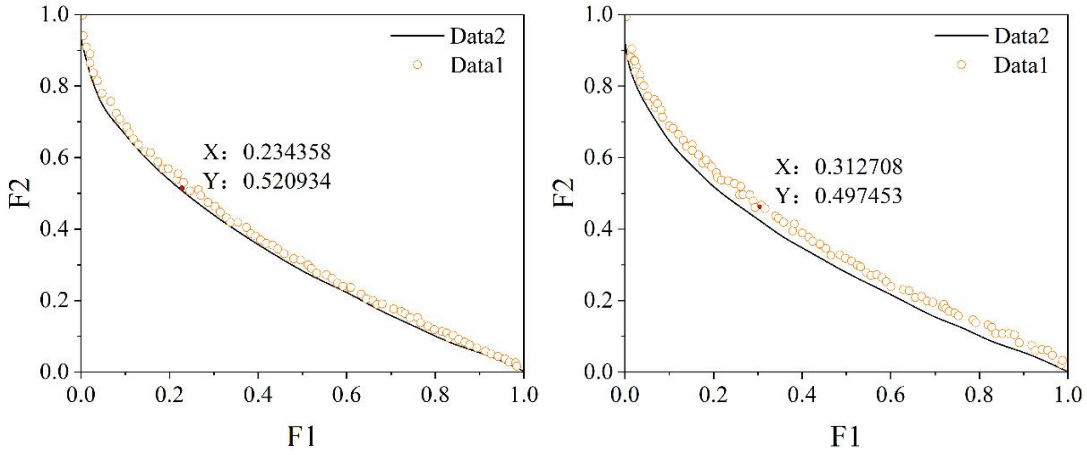

(a) ZDT1 Pareto 1

(b) ZDT1 Pareto 2

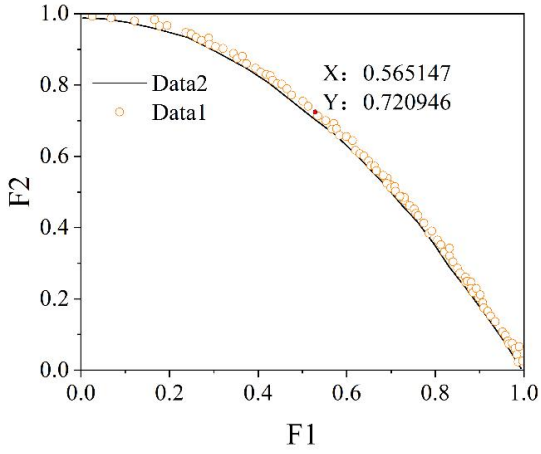

(c) ZDT2 Pareto 1

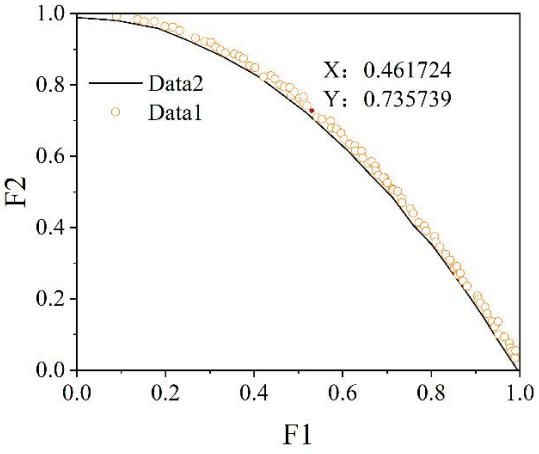

(d) ZDT2 Pareto 2

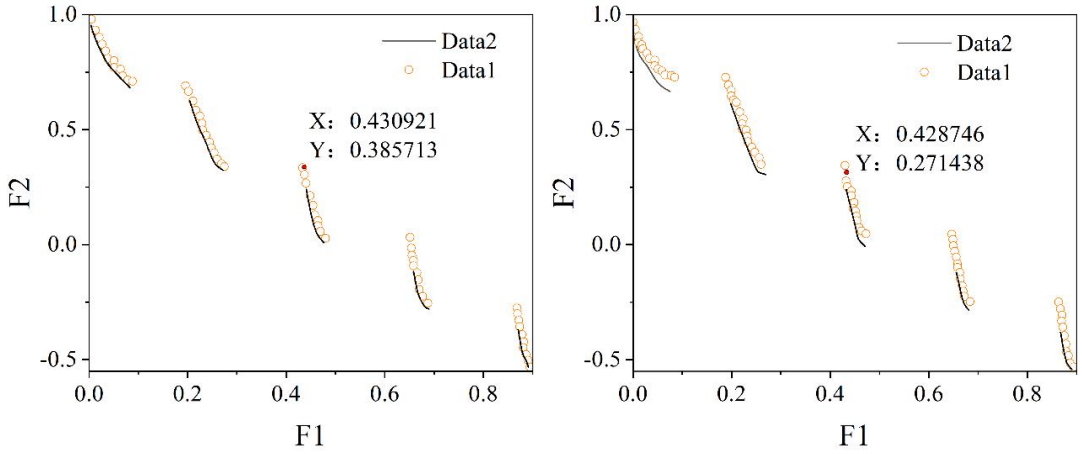

(e) ZDT3 Pareto 1 (f) ZDT3 Pareto 2

Figure 4. Pareto frontier optimization comparison.

(2) Evaluation metrics

The ultimate goal of multi-objective evolutionary algorithm optimization is to obtain a uniform Pareto solution set, in order to qualitatively evaluate the algorithm solution results, the spatial evaluation metrics proposed by Schoot are used. Its definition (e.g., 26):

$$SP = \sqrt{\frac{1}{n-1}\sum_{i=1}^{m}\left(\overline{d} - d_i\right)^2} \tag{26}$$

where: $d_j = \min_j\left(\left|f_1^j(x) - f_1^i(x)\right| + \left|f_2^j(x) - f_2^i(x)\right|\right) i, j = 1 \cdots n$

d is more similar to the crowding distance, being d_i the average of the sum of the spaces occupied by solution i after normalization. After normalization for each object, the distance between the two nearest neighbors of solution i on the j -dimensional objective is computed; m is the number of individuals in the solution set, which is obtained by summing over all k -dimensional objectives for solution m to obtain d_i. The SP is used to denote the uniform distribution of the solution set on the computational boundaries, with the value interval $[0, \infty]$, and the smaller the result of the value indicates the better the distributability.

In testing the comprehensive performance of the multi-objective evolutionary method, it is evaluated using the Inverse Generation Distance (IGD), which means the approximation of the Pareto optimal solution obtained by individual optimization searching to the true Pareto frontier; where P* denotes the ideal frontier of the distribution, and P is the approximate solution. The definition is shown in (27):

$$IGD\left(P^*, P\right) = \frac{\sum_{x \in P^*} \min dis(x, p)}{\left|P^*\right|} \tag{27}$$

Based on the definitions of the above two evaluation index functions, we used four algorithms, NSGA-II algorithm, improved NSGA-II algorithm, MOEA/D-EGO and NMPSO, for comparison; the three selected groups of ZDT functions were calculated independently, and the obtained mean values of SP and IGD are shown in Tables 6 and 7, respectively.

From Table 6, it is concluded that the SP values obtained by the improved NSGA-II algorithm tested in ZDT1 and ZDT2 are significantly lower than the remaining three algorithms, and are closer to the tested values of NMPSO; the low average value in ZDT3 is slightly higher than the tested results of NMPSO algorithm, which is due to the fact that the solution set of ZDT3 has a stepped distribution and has a disconnected portion; in general, from the perspective of the distribution of the improved solutions, the improved NSGA-II algorithm can be compared with the NMPSO algorithm, which is the best choice for the ZDT function. improved distribution of solutions, the improved NSGA-II algorithm has a better performance.

The comparative analysis of the IGDs obtained by each algorithm in Table 7 shows that the improved NSGA-II algorithm is significantly better than the other algorithms. From the data in the table, it can be seen that the average value of the IGDs in the two test functions ZDT1 and ZDT3 is less than 1/2 of that

of the other three algorithms, which indicates that the Pareto optimal solutions obtained by this improved algorithm have a higher degree of convergence.

Table 6. Comparison of SP indicators of different algorithms.

Test function	NSGA-II	NSGA-IIP	MOEA/D-EGO	NMPSO
ZDT1	0.48194	0.29118	0.39723	0.29128
ZDT2	0.45279	0.42614	0.43284	0.44184
ZDT3	0.58782	0.55738	0.57411	0.53284

Table 7. Average value of IGD.

Algorithm	ZDT1	ZDT2	ZDT3
NSGA-II	0.037284	0.074189	0.125780
NSGA-IIP	0.024756	0.039451	0.038374
MOEA/D-EGO	0.047216	0.068292	0.097381
NMPSO	0.049328	0.051474	0.075749

4. Cost-benefit analysis of concrete materials

4.1. Effect of multi-objective optimization with no objective constraint fit ratio

The object of study in this section is an example of raw materials for a given period for a concrete production company in the Pearl River Delta. According to the optimization pathway shown previously, the distribution of the optimal solution dataset obtained after 300 iterative operations is shown in Figure 5. According to the multi-objective program, a total of 200 sets of non-dominated optimal mix ratios were obtained, and the 10 sets of highest rated TOPSIS optimal solutions were searched by TOPSIS scoring. The 10 sets of highest rated TOPSIS optimal solutions found by TOPSIS scoring.

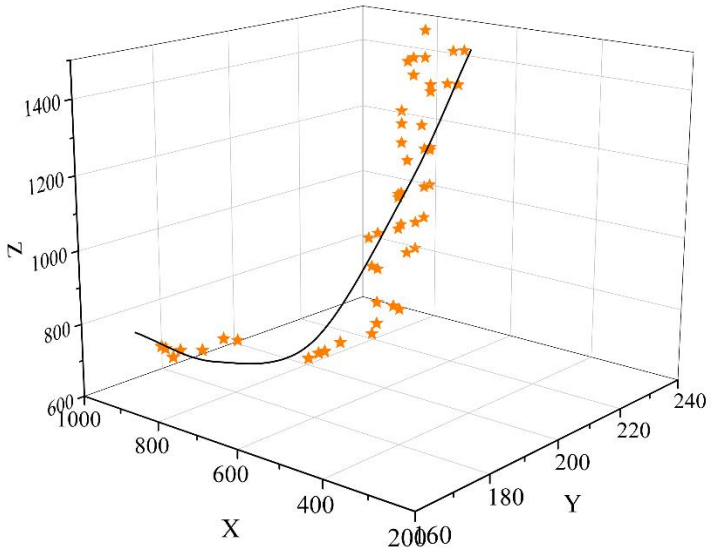

Figure 5. Unconstrained UHPC mix ratio multi-objective optimization solution set position.

4.2. Effect of multi-objective optimization of objective constrained fit ratio

The 10 sets of highest rated TOPSIS optimal solutions found by TOPSIS scoring are shown in Table 8. Comparing the sets of optimal solutions of unconstrained tosopsis (T1) and constrained tosopsis (T2), both of them have higher uniaxial compressive strength than the UHPC standard (120MPa) while the economic cost is less than the selling price of a company in the Pearl River Delta (1,150Yuan/m^3), and at the same time, the carbon emission is less than 1,000g/m^3. The optimization results are relatively successful. However, there is still a slight difference between the two.

Although the uniaxial compressive strength of the optimal solution of the unconstrained set is much higher than the optimal solution of the constrained group, the economic cost of the constrained set shows a clear superiority, and among the solutions with the highest tosis scores of the two types of sets (the

optimal solution of the 10 groups of optimal solutions), the unconstrained solution with the highest tosis scores shows a very high uniaxial compressive strength, as well as a more moderate cost and carbon emission, but comparing the constrained solution with the highest topsis score has a higher economic cost of 398.2 Yuan/m^3 and the Topsisi score of the optimal fitment ratio with constraints is much higher than that of the unconstrained solution, which is close to 0.258. Therefore, the optimal solution can be targeted to seek the optimal solution by restricting the ranges of some of the objective functions without affecting the construction conditions. The combined performance of other objective functions can be increased. The multi-objective optimization model with constrained objective functions within the construction specification in real construction may be more capable of obtaining the ideal fit ratio.

Table 8. TOPSIS optimal solution of UHPC mix ratio multi-objective optimization without target constraint.

Cement content	Total aggregate content	Water content	Fly ash content	Limestone powder content	Uniaxial compressive strength	Prime cost	carbon emission	Topsis score
0.260	0.021	0.105	0.228	0.151	158.765	425.573	891.674	0.95272
0.270	0.021	0.106	0.127	0.151	151.276	426.184	917.194	0.93587
0.260	0.021	0.104	0.228	0.151	158.843	449.763	889.674	0.91993
0.280	0.057	0.106	0.228	0.039	180.618	439.513	945.274	0.91547
0.250	0.068	0.106	0.096	0.151	159.28	453.078	881.097	0.91481
0.250	0.068	0.106	0.118	0.151	158.817	455.289	884.033	0.91125
0.250	0.068	0.106	0.118	0.151	158.453	455.289	884.033	0.91099
0.270	0.057	0.106	0.118	0.151	158.955	456.379	946.285	0.88816
0.270	0.057	0.106	0.118	0.151	158.943	456.379	946.285	0.88815
0.270	0.057	0.106	0.118	0.151	158.943	456.379	946.285	0.88815

5. Conclusion

((1) The study applies the response surface method, selects three factors, namely, water-cement ratio, recycled brick aggregate substitution rate, and volume fraction of polypropylene fiber, and designs a multi-objective optimization model based on the Box-Behnken principle of the response surface method for the prediction of flexural strength, compressive strength, and wear. The values of the model correction coefficient of determination were 0.9725, 0.9645 and 0.9655, respectively, and the P-value was less than 0.01, indicating that the model fit is good, and the fitting accuracy of the model is high, and it can more accurately describe the relationship between the factors and evaluation indexes.

(2) The response surface plot shows that the degree of influence of BF volume doping on flexural strength is greater than that of BF length; the degree of influence of BF length and volume doping on split tensile strength is similar; the degree of influence of BF length on compressive strength is greater than that of BF volume doping.

(3) An improved non-dominated sorting genetic algorithm (I-NSGA-II) is proposed in this paper. In order to test the superiority of the improved NSGA-II algorithm, we start from the convergence speed of the optimization, the uniformity of the distribution of the solution, and introduce the SP and IGD indexes, and test it with the classical three ZDT functions, and the results show that the values of SP and IGD indexes of the improved NSGA-II algorithm are much lower than those of other algorithms, and it exhibits a good solution accuracy in the optimization search.

(4) The economic cost assessment and life cycle assessment of each material of concrete, the design of the unilateral economic cost and unilateral carbon emission cost function, and the introduction of the objective constraints, the use of the improved NSGA-II algorithm to find 200 groups of no objective constraints and constraints on the uniaxial compressive strength of 140-160, respectively, the optimal solution set of the Pareto, and find the optimal solution set of 140-160 by using the tosopsis. Ten sets of optimal solutions are provided as reference for UHPC compatibility ratios in practical engineering. It is found that it is easier to get the ideal solution after constraining the objective function.

References

1. Smarzewski, P., & Stolarski, A. (2022). Properties and performance of concrete materials and structures. Crystals, 12(9), 1193.
2. Golewski, G. L. (2019). Physical characteristics of concrete, essential in design of fracture-resistant, dynamically loaded reinforced concrete structures. Material Design & Processing Communications, 1(5), e82.

3. Valente, M., Sibai, A., & Sambucci, M. (2019). Extrusion-based additive manufacturing of concrete products: revolutionizing and remodeling the construction industry. Journal of composites science, 3(3), 88.
4. Hafizyar, R., & Hunar Dheyaaldin, M. (2019). Concrete technology and sustainably development from past to future. Sustainable Structures and Materials, An International Journal, 2, 1-13.
5. Barbhuiya, S., Das, B. B., Adak, D., Kapoor, K., & Tabish, M. (2025). Low carbon concrete: Advancements, challenges and future directions in sustainable construction. Discover Concrete and Cement, 1(1), 1-24.
6. Demissew, A. (2022). Comparative Analysis of Selected Concrete Mix Design Methods Based on Cost-Effectiveness. Advances in Civil Engineering, 2022(1), 4240774.
7. Khalaf, M. A., Ban, C. C., & Ramli, M. (2019). The constituents, properties and application of heavyweight concrete: A review. Construction and building materials, 215, 73-89.
8. Amran, M., Murali, G., Makul, N., Tang, W. C., & Alluqmani, A. E. (2023). Sustainable development of eco-friendly ultra-high performance concrete (UHPC): Cost, carbon emission, and structural ductility. Construction and Building Materials, 398, 132477.
9. Santamaria, J., & Valentin, V. (2018). Perceptions on construction-related factors that affect concrete quality, costs and production. Avances en Ciencias e Ingenierias, 10(1), 120-139.
10. Skrzypczak, I., & Słowik, M. (2019). Economical aspects concerning quality control of concrete. Budownictwo i Architektura, 18(1).
11. Gallardo, R., & Elevado, K. J. (2018). Cost-benefit analysis of concrete mixed with waste ceramic tiles and fly ash. Proc. WOW Concr, 1-10.
12. Ohemeng, E. A., & Ekolu, S. O. (2020). Comparative analysis on costs and benefits of producing natural and recycled concrete aggregates: A South African case study. Case Studies in Construction Materials, 13, e00450.
13. Han, Y., Meng, L. Y., Lin, R., Kim, S., Kim, T., & Wang, X. Y. (2024). Evaluating the sustainability of microwave pre-cured high-volume slag concrete: Mechanical properties, environmental impact and cost-benefit analysis. Journal of Building Engineering, 96, 110663.
14. Awchat, G. D. (2021). Cost-benefit analysis of using recycled coarse aggregate in plain and fiber reinforced concrete. Advances in Science and Technology. Research Journal, 15(3), 233-242.
15. Sabbaghzade Feriz, A., Varaee, H., & Ghasemi, M. R. (2024). Multi-Objective Optimization in Support of Life-Cycle Cost-Performance-Based Design of Reinforced Concrete Structures. Mathematics, 12(13), 2008.
16. Panesar, D. K., Kanraj, D., & Abualrous, Y. (2019). Effect of transportation of fly ash: Life cycle assessment and life cycle cost analysis of concrete. Cement and Concrete Composites, 99, 214-224.
17. Alqahtani, F. K., Abotaleb, I. S., & ElMenshawy, M. (2021). Life cycle cost analysis of lightweight green concrete utilizing recycled plastic aggregates. Journal of Building Engineering, 40, 102670.
18. Dong, Y. (2018). Performance assessment and design of ultra-high performance concrete (UHPC) structures incorporating life-cycle cost and environmental impacts. Construction and Building Materials, 167, 414-425.
19. Renne, N., Kara De Maeijer, P., Craeye, B., Buyle, M., & Audenaert, A. (2022). Sustainable assessment of concrete repairs through life cycle assessment (LCA) and life cycle cost analysis (LCCA). Infrastructures, 7(10), 128.
20. Adamu, M., & Ibrahim, Y. E. (2024). Environmental sustainability and cost-benefit analysis of concrete containing date palm ash and eggshell powder: A response surface methodology approach. Case Studies in Chemical and Environmental Engineering, 9, 100636.
21. Jhatial, A. A., Kumar, A., Bheel, N., Sohu, S., & Goh, W. I. (2022). Assessing the sustainability and cost-effectiveness of concrete incorporating various fineness of eggshell powder as supplementary cementitious material. Environmental Science and Pollution Research, 29(56), 84814-84826.
22. Makul, N. (2020). Cost-benefit analysis of the production of ready-mixed high-performance concrete made with recycled concrete aggregate: A case study in Thailand. Heliyon, 6(6).
23. Gheibi, M., Karrabi, M., Shakerian, M., & Mirahmadi, M. (2018). Life cycle assessment of concrete production with a focus on air pollutants and the desired risk parameters using genetic algorithm. Journal of environmental health science and engineering, 16(1), 89-98.
24. Naseri, H. (2019). Cost optimization of no-slump concrete using genetic algorithm and particle swarm optimization. International Journal of Innovation, Management and Technology, 10(1), 33-37.
25. Gao, J., Ozbay, K., Nassif, H., & Kalan, O. (2019). Stochastic Multi-Objective Optimization-Based Life Cycle Cost Analysis for New Construction Materials and Technologies. Transportation Research Record, 2673(11), 466-479.
26. Tavares, C., & Grasley, Z. (2022). Machine learning-based mix design tools to minimize carbon footprint and cost of UHPC. Part 2: Cost and eco-efficiency density diagrams. Cleaner Materials, 4, 100094.
27. Aydın, Y., Cakiroglu, C., Bekdaş, G., Işıkdağ, Ü., Kim, S., Hong, J., & Geem, Z. W. (2023). Neural network predictive models for alkali-activated concrete carbon emission using metaheuristic optimization algorithms. Sustainability, 16(1), 142.
28. Haigh, R., Bouras, Y., Sandanayake, M., & Vrcelj, Z. (2023). Economic and environmental optimisation of waste cardboard kraft fibres in concrete using nondominated sorting genetic algorithm. Journal of Cleaner Production, 426, 138989.
29. Ahmadi-Nedushan, B., & Almaleeh, A. M. (2024). MATERIAL COST OPTIMIZATION OF ONE-WAY REINFORCED CONCRETE SLABS USING AN ELITIST GENETIC ALGORITHM: A SENSITIVITY ANALYSIS BASED ON ACI 318-19. Int. J. Optim. Civil Eng, 14(4), 573-593.
30. Lv, H., Du, M., Li, Z., Xiao, L., & Zhou, S. (2024). Cost optimization of graphene oxide-modified ultra-high-performance concrete based on machine learning methods. Inorganics, 12(7), 181.

31. Elmasry, N. H., & Elshaarawy, M. K. (2025). Hybrid metaheuristic optimized Catboost models for construction cost estimation of concrete solid slabs. Scientific Reports, 15(1), 21612.
32. Riffat Islam,Md. Bashar Uddin,Mohammad Rashel Hawlader & Ahmed Jalal Uddin. (2025). Employing response surface methodology in the production of sustainable PC yarn from recycled polyester and recycled cotton.Cleaner Waste Systems,12,100421-100421.https://doi.org/10.1016/J.CLWAS. 2025. 100421.
33. Satyabrat Sahoo,Satya Prakash Sahoo,Ram Chandra Barik & Manas Ranjan Kabat. (2025). An entropy weight-non dominated sorting genetic algorithm for QoS resource optimization in 5G driven IoV networks.Wireless Networks,31(6),1-17.https://doi.org/10.1007/S11276-025-03989-1.